

Modulating anionic activities in layered Li-rich cathode materials with inverse spinel MnFe_2O_4 coating

Liying Bao^{1,2}, Xinyu Zhu^{1,2}, Ning Li^{1,2,*}, Yongjian Li^{1,2}, Lifeng Xu^{1,2}, Lai Chen^{1,2}, Duanyun Cao^{1,2}, Yun Lu^{1,2}, Yuefeng Su^{1,2,*}, Youyou Fang^{1,2}, Chenxing Yang^{1,2}, Ran An^{1,2}

¹ Beijing Key Laboratory of Environmental Science and Engineering, School of Material Science and Engineering, Beijing Institute of Technology, Beijing 100081, China

² Beijing Institute of Technology Chongqing Innovation Center, Chongqing, 401120, China

Abstract: Layered Li-rich cathode oxides can provide high specific capacity due to oxygen anion redox involving in charge compensation process during cycling, but there is a severe structural transition from layered to spinel accompanying with irreversible oxygen loss during cycling, which lead to electrochemical degradation. The current researches show that the irreversible oxygen evolution reaction of layered lithium-rich materials in the first cycle mainly comes from the surface lattice oxygen, so the surface modification by the materials with more stable structure is one of the effective ways to improve the electrochemical performance of layered lithium-rich materials. In this paper, we report a modified layered lithium-rich cathode material by surface coating of inverse spinel MnFe_2O_4 . The inverse spinel has strong polarization effect on anion migration due to its different atoms occupying octahedral sites from layered structure and it can also modulate the Fermi level and stretching the O-O bond, thereby increasing the energy barrier for surface oxygen oxidization. Furthermore, the three-dimensional connected tunnel structure of the inverse spinel also makes the surface layer of the material have a faster lithium ion transferring rate, and a large number of lithium storable vacancies inside of it improved the Li^+ intercalation efficiency, initial coulombic efficiency and rate performance. Compared with the unmodified sample, the modified material coated with 2% MnFe_2O_4 has superior cycle stability and outstanding rate performance. It is hoped our work would provide the knowledge for the future development of high-performance cathode materials for Li-ion batteries.

1. Introduction

Layered Li-rich oxides have become one of the most promising cathode candidates for next-generation high-energy-density Li-ion batteries due to their high specific discharge capacity (250 mAh/g) and low cost as well as environmental benignity. Different from the traditional layered cathode materials, such as LiCoO_2 and NCM cathode materials, where the capacities are mainly provided by transition metal redox for charge compensation, the additional high specific capacity of layered lithium-rich cathode materials mainly comes from the anionic oxygen redox ($\text{O}^{2-/n}$)[1-3]. However, a major bottleneck in the practical application of layered lithium-rich cathode materials is the severe capacity and voltage fade, caused by the irreversible migration of transition metal ions leading to phase transform from layered to the spinel structure during cycling[4]. In addition, the side reaction occurs in the electrode and the electrolyte, and the oxygen evolution at surface caused by the deep oxidation of anionic oxygen, are the two other important reasons for the failure of the layered lithium-rich cathode material. At present, researchers have developed various surface protective layers to reduce the side reactions occurs in the electrode and the electrolyte and slow down

the erosion of the electrode material by the electrolyte, including oxides (Al_2O_3 [5], TiO_2 [6], ZrO_2 [7]), phosphates (AlPO_4 [8], Li_3PO_4 [9], LiFePO_4 [10]) and fluorides (AlF_3 [11], LiF [12], MgF_2 [13]). However, the oxygen evolution caused by the deep oxidation of anionic oxygen still remains, which can not only bring about the safety problem of the battery, but also reduce the coulombic efficiency in the first cycle. More importantly, it can also deteriorate surface mass and charge transfer during the subsequent electrochemical reaction, thus, it is crucially needed to regulate the oxygen activities for the layered Li-rich materials.

The oxygen evolution reaction during initial charging process of the layered lithium-rich cathode material mainly includes the following processes: First, the undercoordinated Li-O bonds and the TM-O bonds near surface are broken, and then a large number of oxygen anions migrate to the surface and lose electrons to form new O-O bonds and release oxygen[14-15]. Therefore, to inhibit oxygen evolution of layered lithium-rich cathode materials, we can increase the binding energy of TM-O through surface doping with high-electronegative transition metal elements, thus making oxygen evolution thermodynamically difficult. At the same time, preventing the migration of oxygen ions to the surface is the second

* Corresponding author: ningli@bit.edu.cn

effective way to alleviate the oxygen evolution of layered lithium-rich cathode, and the migration process of anions is related to the effect of the external electric field[16, 17] and the formation of oxygen vacancies on the surface during synthesis and cycling[18]. Therefore, the driving force for the migration of oxygen anions can be weakened by coating the dielectric polarized materials on the surface of layered lithium-rich cathode material; and reducing the oxygen vacancies on the surface of the material by optimizing synthesis process. Since both layered lithium-rich oxides and spinel oxides belongs to cubic oxygen close-packing structure[19-21] and Mn-based spinel oxides are also widely used to catalyze the oxygen reduction reaction, so spinel oxides can be used as the coating agents to improve the cycle stability, rate capability, and most importantly to reduce the irreversible oxygen release of layered lithium-rich cathode materials. In general, spinel can be written as $\{A\}[B_2]X_4$ which is a cubic close-packed structure consisting of X^{2-} ions. A atom occupies tetrahedral positions and B atom occupy octahedral positions. If the A atoms exchange positions with half of the B atoms, then $\{A\}[B_2]X_4$ would transform from an ortho-spinel structure to an inverse-spinel structure— $\{B\}[AB]X_4$ [22, 23]. In the Mn-Fe-based spinel, Mn atoms and half of Fe atoms co-occupy the octahedral sites, and the other half of Fe atoms occupy tetrahedral sites. Here, we report a co-precipitation method to build a $MnFe_2O_4$ coating layer on the surface of Li-rich layered oxide after annealing at 550 °C. Through systematically electrochemical and structural characterization, it is confirmed that $MnFe_2O_4$ has been successfully coated on surface of layered Li-rich cathode $Li_{1.2}Mn_{0.6}Ni_{0.2}O_2$ (labeled as LMO), and this coating modification can greatly enhance the initial coulombic efficiency, reducing the irreversible oxygen loss, and improving the cycle stability and rate performance. It is hoped this work should shed the light on the future cathode materials modification for advanced Li-ion batteries.

2. Experiment

Synthesis of $Li_{1.2}Mn_{0.6}Ni_{0.2}O_2$: According to the chemical formula, the stoichiometric metal salts $LiC_2H_3O_2 \cdot 2H_2O$, $MnC_4H_6O_4 \cdot 4H_2O$, $NiC_4H_6O_4 \cdot 4H_2O$ were weighed (5% excess of lithium salt), then deionized water was added and the mixture was stirred to form a clear solution. In addition, the citric acid was dissolved into deionized water and added in the mixture, and the ammonia was added to adjust the pH to 7. Finally, the mixture solution was heated at 80 °C until to form a green gel. The obtained gel was scraped and dried in an oven, and then calcined in a muffle furnace at 450 °C for 5 hours and at 900 °C for 12 hours with a heating rate of 5 °C/minute.

Spinel $MnFe_2O_4$ coating modification: 1.0 gram of the pristine LMO material was dispersed in deionized water, which is marked as solution A. Then stoichiometric anhydrous $FeCl_3$ and $MnSO_4 \cdot H_2O$ were dissolved in deionized water with stirring, which is marked as solution B. The solution B was dropwise added into the solution A and stirred uniformly. Then NaOH was added to -adjust

pH value to ~ 11, and after reacting for 2 hours, the mixed solution was then centrifuged and dried in an oven. Finally, the dry powder was calcinated in a muffle furnace at 550 °C for 5h with heating rate of 5 °C/min.

Structure characterization and electrochemical tests: The crystal structure of the sample was characterized by X-ray diffraction (XRD), $2\theta = 10\text{--}90^\circ$, $10^\circ/\text{min}$, step size of 0.02° . The morphology and elemental composition of the samples was characterized by scanning electron microscopy (SEM-EDS). All samples were assembled into a coin cell with using lithium metal as the anode, where the electrode was the uniform mass mixture for the ratio of 8(active material):1(acetylene black):1(PVDF). Here, the average mass loading of the active cathode material on carbon-coated aluminum foil is 2.0~3.0 mg/cm^2 . The cathodes and anodes are separated by two two Celgard 2500films, and 1 mol $LiPF_6$ was dissolved in EC/DEC (1:1 v/v) as the electrolyte. The cells were cycled by a LAND device at 30 °C between 2–4.8 V (nominal specific capacity of 250 mAh/g).

3. Results and discussion

In order to characterize the structure of layered lithium-rich cathode material before and after coating, the XRD patterns of all the samples were collected. Figure 1 shows the X-ray diffraction patterns of the as-synthesized pristine material LMO and the modified materials with coating ratios (molar ratio) of 1.5%, 2%, and 4% (labeled as LMO1.5, LMO2, and LMO4). It can be seen that all the patterns of the pristine layered lithium-rich material can be well indexed with layered structure with R3-m symmetry, except the superlattice peak at 20-25° which is related to the $LiMn_6$ or $LiMn_5Ni$ ordering in the TM slabs [24, 25]. The diffraction peaks of the three modified samples are similar to the pristine material LMO, indicating that the crystal structures of the modified samples have not changed significantly after surface coating. However, the LMO1.5 sample has an obvious spinel structure impurity phase, and the super-lattice peaks of the three modified samples near 20-25 ° gradually weaken with the increasing of the coating amount. The decreasing of intensity ratio I003/I104 (LMO-1.31, LMO1.5-1.33, LMO2-1.14, LMO4-1.21) of the modified samples also indicates the increasing in the degree of Li/Ni mixing after surface coating, while the appropriate Li/Ni mixing may stabilize the layered structure and the improve the cycle stability.

Figure 2 shows the scanning electron microscope (SEM) images of the pristine LMO and the sample with a coating amount of 2%. The morphologies of all samples present as 100-300 nm primary particles with different degree of agglkomeration. It can be seen from Fig.2a that as the coating amount increases, the surface of primary particles gradually becomes rough, which indicates that the surface of the material is successfully covered by coating agent. In order to investigate the uniformity of coating, we performed EDS mapping tests on the pristine material LMO(Fig.2b) and the modified material LMO2(Fig.2c). The EDS mapping results show that in the pristine material LMO, Mn, Ni and O are uniformly dispersed. As

for the modified sample LMO2, the Fe, Mn and Ni are uniform dispersed as well. It can be concluded that the coating layer has been successfully coated on the surface of the LMO sample.

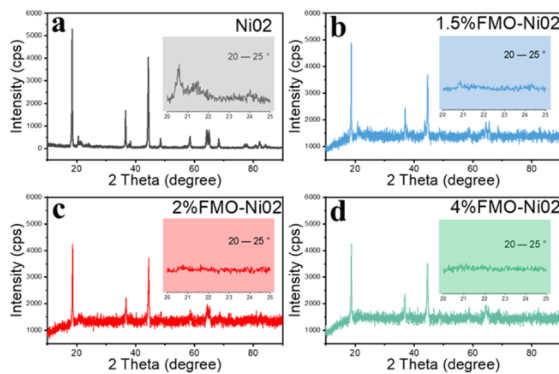


Figure 1. XRD pattern of the four samples; (a)—LMO pristine; (b)—LMO1.5; (c)—LMO2; (d)—LMO4.

In order to investigate the effect of MFO coating on the electrochemical performance of layered Li-rich material, Figure 3 shows the first cycle curve and the corresponding dQ/dV curve of the pristine LMO and the modified samples at a current density of 0.1 C, and Table 1 shows the first charge-discharge electrochemical data. It can be seen that the LMO, LMO1.5, LMO2 and LMO4 samples can yield initial charge capacities of 326.7 mAh/g, 240.6 mAh/g, 298.4 mAh/g, and 273.7 mAh/g, and the gradual decrease of charge capacity with the increase of MFO coating, indicates that the initial oxygen release was alleviated. In addition, with the increase of the coating layer, the irreversible capacity in the first cycle can also be effectively reduced and the initial coulombic efficiency is increased from 81.5% of the pristine LMO to 96.4% of LMO4. The initial charge-discharge curves of all samples are shown in Fig. 3a. The charge curves are composed of the slope region and a plateau at around 4.5 V, corresponding to the oxidation peaks of Ni and O respectively as shown in the dQ/dV plots in Fig. 3b. In Figure 3b, there is also an obvious sharp reduction peak around 2.8V, corresponding to the Mn³⁺/Mn⁴⁺ redox couple of the inverse spinel MnFe₂O₄ structure. Combined with the EDS spectrum, it further confirms that the inverse spinel MnFe₂O₄ is successfully coated on the surface of the material. More importantly, it can be seen that with increasing of coating amount, the potential of the plateau increases, corresponding to the right shift of O oxidation peak in the dQ/dV plots (Fig. 3b). This phenomenon infers that the oxidation of oxygen becomes difficult, that is, the irreversible release of oxygen is alleviated.[22, 23]It is believed that the inverse spinel MnFe₂O₄ coating layer promotes the charge polarization effect and prevent the migration of oxygen anion to surface. Meanwhile, the inverse spinel has stronger binding energy to oxygen anion to prevent the formation of the O-O dimer at the surface. Therefore, the coating of inverse spinel MnFe₂O₄ alleviate the oxygen evolution reaction both kinetically and thermodynamically. In addition, lithium-deficient spinel MnFe₂O₄, can provide lithium ion vacancies to accommodate many extra lithium ions, and thus improve the initial coulombic efficiency. The discharge curve of

the sample is a gradually decreasing slope. It can be seen an obvious plateau appears below the discharge 3.0 V among the LMO2 and LMO4 samples.

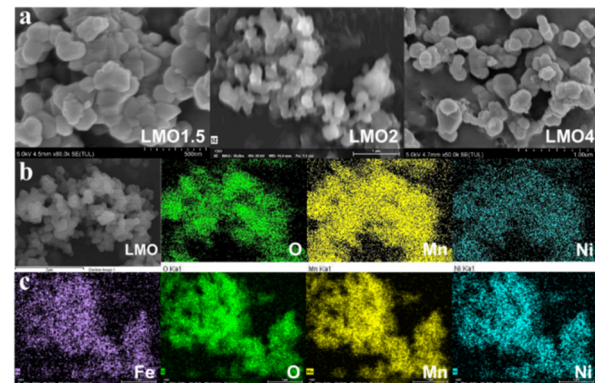


Figure 2. (a)SEM patterns of the modified samples; (b)SEM patterns and corresponding EDS spectroscopy of LMO; (c)EDS spectroscopy of LMO2.

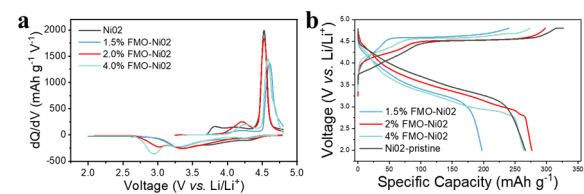


Figure 3. The first charge-discharge curves of the four samples (b) and corresponding dQ/dV curves (a).

Table 1. The electrochemical data of first cycle for the four samples.

	Charge capacity mAh/g	Discharge capacity mAh/g	ICE	Irreversible capacity mAh/g
LMO1.5	240.6	197.4	82.06%	43.2
LMO2	298.4	276.9	92.82%	21.5
LMO4	273.7	263.8	96.37%	9.9
LMO-NiO2	326.7	266.4	81.52%	60.3

Figure 4 shows the charge-discharge curves of the pristine LMO and the modified samples under 0.1 C current density for 50 cycles. With the increase of cycling number, all samples show capacity decay. The discharge capacity of the pristine material LMO decreased from 266.4 mAh/g to 194.6 mAh/g after 50 cycles, and the capacity retention is only 73.5%. Among the modified samples, the LMO1.5 sample did not form a good coating structure and showed rapid capacity decay and poor capacity retention while the LMO2 and LMO4 samples shows outstanding cycle performance. The LMO2 sample shows the best capacity retention, from the initial capacity of 276.9 mAh/g to the 236.9 mAh/g after 50 cycles with capacity retention of 85.6%. In addition, a small plateau around 2.8 V remains on the discharge curves of LMO2 and LMO4 samples, indicating the formation of a stable inverse spinel structure coating layer[26, 27].

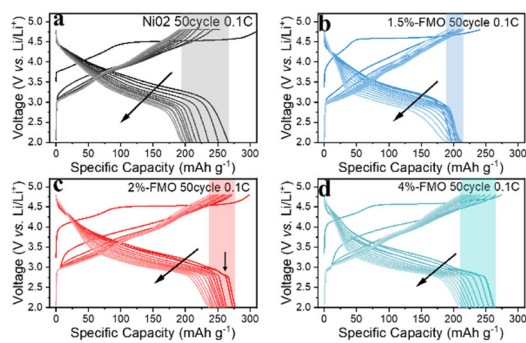


Figure 4. The charge-discharge curves of 50 cycles at a current density of 0.1 C (a) LMO, (b) LMO1.5, (c) LMO2, (d) LMO4.

In order to study the effect of the inverse spinel coating on the rate performance of the material, Figure 6 shows the rate performance test of all the samples at different current densities. Under 0.3 C, 0.5 C, 1 C, 3 C, 5 C and 10 C rates, the pristine LMO shows discharge capacities of 218 mAh/g, 206 mAh/g, 190 mAh/g, 149 mAh/g, 110 mAh/g, 38 mAh/g, respectively. After surface coating with the Li^+ conductive inverse spinel, the modified samples display superior rate performance. The LMO2 sample shows the best rate performance, and exhibits discharge specific capacities of 257 mAh/g, 252 mAh/g, 243 mAh/g, 218 mAh/g, 189 mAh/g, and 113 mAh/g at the current density of 0.3 C, 0.5 C, 1 C, 3 C, 5 C, 10 C, respectively. It is indicated that the inverse spinel structure can provide a three-dimensional lithium ion transport channel, which accelerates the interfacial lithium ions mass transfer from the electrode to the electrolyte.

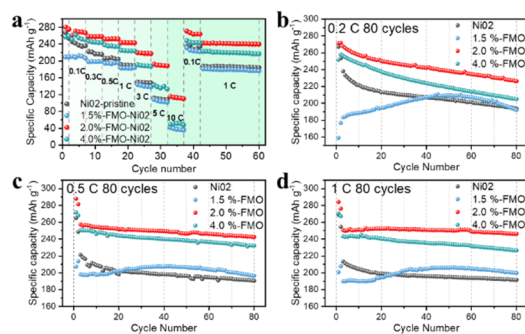


Figure 5. (a) The rate performance of the four samples; (b-d) The discharge capacity curves of the four samples at the current density of 0.2 C, 0.5 C and 1 C for 80 cycles. Figures 5b-d shows the rate cycling performance of all the samples at 0.2 C, 0.5 C and 1 C. At different rate, except for that of LMO1.5, the capacities of all other samples gradually decrease with the cycling number. The modified samples LMO2 and LMO4 show much higher capacity and capacity retention than the pristine materials at all different rates. As shown in Fig. 6b-d, the pristine LMO have initial capacities of 238 mAh/g, 221 mAh/g and 213 mAh/g at 0.2 C, 0.5 C, and 1 C, respectively. After 80 cycles, it shows the discharge capacity of 194 mAh/g, 191 mAh/g and 192 mAh/g with the capacity retention are 81.5%, 86.4%, and 90.1%, respectively. After modification, the initial capacities of the sample LMO2 greatly increase to 267 mAh/g, 257 mAh/g, 251 mAh/g at

0.2 C, 0.5 C, and 1 C, respectively. And after 80 cycles it shows the capacities of 226 mAh/g, 242 mAh/g and 246 mAh/g with the capacity retention are 84.6%, 94.2%, and 98.0%. The significant enhancement in the discharge specific capacity and capacity retention of the modified materials is mainly due to that the stable inverse spinel coating structure on the surface enables the substantial improvement in the lithium ion conductivity of the material. In addition, it can be seen that the excess inverse spinel coating would not further increase the rate performance, which can be attributed to that the obtained incompletely crystallized inverse spinel coating would increase the surface charge transfer resistance by low-temperature processing. Therefore, only a suitable coating amount can optimize the rate performance of lithium-rich manganese-based cathode material.

4. Conclusion

In summary, we have successfully prepared MnFe_2O_4 inverse spinel-coated layered Li-rich cathode materials, and electric field effect of the inverse spinel surface coating layer can suppress the outward migration of O anions, and its stronger binding energy to oxygen anion can also slow down the anion migration and oxygen gas release. In addition, the oxygen oxidation reaction in the first cycle become thermodynamically difficult and its kinetic has been enhanced after coating. With these merits of inverse spinel surface coating, the layered Li-rich cathodes show greatly reduced the irreversible initial capacity and improved initial coulombic efficiency (LMO2-92.82%, LMO-81.52%), and the LMO2 sample shows best capacity retention of 85.6% capacity retention after 50 cycles at 0.1C and outstanding rate capability of 267 mAh/g, 257 mAh/g, 251 mAh/g at 0.2 C, 0.5 C, and 1 C with high capacity retention). Our results suggest surface coating with inverse spinel enable to tune the oxygen activities in Li-rich layered oxides, and such finding should provide valuable knowledge for development of the high-performance cathode materials for the next-generation Li-ion batteries.

Acknowledgements

This work was supported by National Key R&D Program of China 2021YFC2902905, Chongqing Talents Plan for Young Talents CQYC202005032, National Natural Science Foundation of China (22109010, 21875022, 22179008), N. Li, L. Chen and D. Cao acknowledge the support from Beijing Institute of Technology Research Fund Program for Young Scholars.

References

- Assat, G.; Tarascon, J.-M. *Nature Energy* 2018, 3, (5), 373-386.
- Assat, G.; Foix, D.; Delacourt, C.; Iadecola, A.; Dedryvere, R.; Tarascon, J. M. *Nat Commun* 2017, 8, (1), 2219.

3. Rozier, P.; Tarascon, J. M. *Journal of The Electrochemical Society* 2015, 162, (14), A2490-A2499.
4. Ates, M. N.; Jia, Q.; Shah, A.; Busnaina, A.; Mukerjee, S.; Abraham, K. M. *Journal of The Electrochemical Society* 2013, 161, (3), A290-A301.
5. Kobayashi, G.; Irii, Y.; Matsumoto, F.; Ito, A.; Ohsawa, Y.; Yamamoto, S.; Cui, Y.; Son, J.-Y.; Sato, Y. *Journal of Power Sources* 2016, 303, 250-256.
6. Kim, S.-J.; Kim, M.-C.; Kwak, D.-H.; Kim, D.-M.; Lee, G.-H.; Choe, H.-S.; Park, K.-W. *Journal of Power Sources* 2016, 304, 119-127.
7. Wang, Z.; Liu, E.; Guo, L.; Shi, C.; He, C.; Li, J.; Zhao, N. *Surface and Coatings Technology* 2013, 235, 570-576.
8. Wu, F.; Zhang, X.; Zhao, T.; Li, L.; Xie, M.; Chen, R. *ACS Appl Mater Interfaces* 2015, 7, (6), 3773-81.
9. Chen, D.; Zheng, F.; Li, L.; Chen, M.; Zhong, X.; Li, W.; Lu, L. *Journal of Power Sources* 2017, 341, 147-155.
10. He, L.; Xu, J. M.; Wang, Y. J.; Zhang, C. J. *ACTA PHYSICO-CHEMICA SINICA* 2017, 33, (8), 1605-1613.
11. Li, G. R.; Feng, X.; Ding, Y.; Ye, S. H.; Gao, X. P. *Electrochimica Acta* 2012, 78, 308-315.
12. Fu, C.; Wang, J.; Wang, J.; Meng, L.; Zhang, W.; Li, X.; Li, L. *Journal of Materials Chemistry A* 2019, 7, (40), 23149-23161.
13. Sun, S.; Wan, N.; Wu, Q.; Zhang, X.; Pan, D.; Bai, Y.; Lu, X. *Solid State Ionics* 2015, 278, 85-90.
14. Lin, F.; Markus, I. M.; Nordlund, D.; Weng, T.-C.; Asta, M. D.; Xin, H. L.; Doeff, M. M. *Nature Communications* 2014, 5, (1).
15. Strehle, B.; Kleiner, K.; Jung, R.; Chesneau, F.; Mendez, M.; Gasteiger, H. A.; Piana, M. *Journal of The Electrochemical Society* 2017, 164, (2), A400-A406.
16. Hu, E.; Yu, X.; Lin, R.; Bi, X.; Lu, J.; Bak, S.; Nam, K.-W.; Xin, H. L.; Jaye, C.; Fischer, D. A.; Amine, K.; Yang, X.-Q. *Nature Energy* 2018, 3, (8), 690-698.
17. Li, X.; Qiao, Y.; Guo, S.; Xu, Z.; Zhu, H.; Zhang, X.; Yuan, Y.; He, P.; Ishida, M.; Zhou, H. *Adv Mater* 2018, 30, (14), e1705197.
18. Li, Q.; Ning, D.; Zhou, D.; An, K.; Wong, D.; Zhang, L.; Chen, Z.; Schuck, G.; Schulz, C.; Xu, Z.; Schumacher, G.; Liu, X. *Journal of Materials Chemistry A* 2020, 8, (16), 7733-7745.
19. Peng, J.; Li, Y.; Chen, Z.; Liang, G.; Hu, S.; Zhou, T.; Zheng, F.; Pan, Q.; Wang, H.; Li, Q.; Liu, J.; Guo, Z. *ACS Nano* 2021.
20. Zhang, W.; Sun, Y.; Deng, H.; Ma, J.; Zeng, Y.; Zhu, Z.; Lv, Z.; Xia, H.; Ge, X.; Cao, S.; Xiao, Y.; Xi, S.; Du, Y.; Cao, A.; Chen, X. *Adv Mater* 2020, 32, (19), e2000496.
21. Luo, D.; Ding, X.; Fan, J.; Zhang, Z.; Liu, P.; Yang, X.; Guo, J.; Sun, S.; Lin, Z. *Angew Chem Int Ed Engl* 2020, 59, (51), 23061-23066.
22. Béjar, J.; Álvarez-Contreras, L.; Ledesma-García, J.; Arjona, N.; Arriaga, L. G. *Journal of Electroanalytical Chemistry* 2019, 847.
23. Li, C.; Han, X.; Cheng, F.; Hu, Y.; Chen, C.; Chen, J. *Nat Commun* 2015, 6, 7345.
24. Wang, G.; Yi, L.; Yu, R.; Wang, X.; Wang, Y.; Liu, Z.; Wu, B.; Liu, M.; Zhang, X.; Yang, X.; Xiong, X.; Liu, M. *ACS Appl Mater Interfaces* 2017, 9, (30), 25358-25368.
25. Hy, S.; Felix, F.; Rick, J.; Su, W. N.; Hwang, B. J. *J Am Chem Soc* 2014, 136, (3), 999-1007.
26. Eum, D.; Kim, B.; Song, J. H.; Park, H.; Jang, H. Y.; Kim, S. J.; Cho, S. P.; Lee, M. H.; Heo, J. H.; Park, J.; Ko, Y.; Park, S. K.; Kim, J.; Oh, K.; Kim, D. H.; Kang, S. J.; Kang, K. *Nat Mater* 2022.
27. Pei, Y.; Xu, C. Y.; Xiao, Y. C.; Chen, Q.; Huang, B.; Li, B.; Li, S.; Zhen, L.; Cao, G. *Advanced Functional Materials* 2017, 27, (7).